JOURNAL OF MATERIALS SCIENCE 24 (1989) 3069–3075

Effect of phosphorus and silicon addition on the sintered properties of 316L austenitic stainless steel and its composites containing 4 vol % yttria

SOHAN LAL, G. S. UPADHYAYA
Department of Metallurgical Engineering, Indian Institute of Technology, Kanpur 208 016, India

Up to 2 mass % phosphorus and 5 mass % silicon were added by a premix route to 316L austenitic stainless steel and its 4 vol % yttria-containing composites. Sintering was carried out at 1100 and 1300° C, respectively, for 1 h in hydrogen. Sintered properties such as linear and radial shrinkages, sintered density, densification parameter and porosities, were measured. Corrosion behaviour by complete immersion in 1 N H_2SO_4 and mechanical properties of sintered MPIF (Metal Powder Industries Federation) test pieces were also evaluated. A greater improvement in densification behaviour was found for phosphorus addition than for silicon after sintering at 1300° C. However, better corrosion resistance was shown after silicon addition than after phosphorus. Optimum ultimate tensile strength and per cent elongation were observed at 1 mass % phosphorus and 4 mass % silicon compositions. Results have been interpreted on the basis of δ-ferrite stabilization in 316L by such additions.

1. Introduction

316L austenitic stainless steel (γSS) is one of the most common grades of stainless steel and therefore many reports of its sintered properties are available. Elements such as molybdenum, phosphorus and silicon, which stabilize the ferrite phase [1–4], can be added to γSS by either prealloying or premixing routes in order to modify the properties of the single-phase steel.

Reports suggest that the addition of these elements to stainless steel P/M (powder metallurgy) parts enhances the sintering rate. The reasons for such an enhanced sintering are: (i) the presence of a liquid phase, and (ii) the volume diffusivity which is many times higher in the body centred cubic ferrite phase than in the face centred cubic austenite phase.

The use of phosphorus to activate the sintering of ferrous alloys by liquid-phase sintering has been reported extensively [5–7]. White [6] reported that phosphorus addition as ferrophosphorus to γSS by a premixing route improved dimensional changes considerably. It was further reported that tensile strength, yield strength, hardness, per cent elongation and sintered density increased with increasing phosphorus content up to 6% in γSS.

Sands and Watkinson [8] have shown that variations in composition have a marked effect on densification behaviour during sintering, and in particular, the addition of silicon and molybdenum to an 18% Cr–10% Ni steel powder has a substantial effect. Shrinkage increased when silicon content was increased or when molybdenum and/or niobium were present in the austenitic stainless steel, but the green density was adversely affected. Stainless steel P/M compacts containing ferrite-stabilizing elements exhibited higher sintered density at a temperature when steel was normally austenitic. Shaw and Honeycombe [9] have reported the formation of δ-ferrite and an increased rate of sintering of 316L grade austenitic stainless steel as a result of crystal structure change. It was also reported that the reduction of nickel content of stainless steel powder increased the sintering rate, even in the fully austenitic condition.

Wang and Su [10] studied the effect of the addition of silicon powder by a premixing route to 304L stainless steel powder and reported the appearance of liquid phase, because of contact melting at a temperature well below the melting points of the powder constituents, which ultimately resulted in rapid solidification. It was also reported [11] that the introduction of silicon into P/M austenitic stainless steel improved hardness and tensile strength, but reduced ductility. Wen-Feng [12] mixed up to 5 mass % silicon powder with the austenitic stainless steel and studied its effect on sintering behaviour, microstructure, and physical and mechanical properties. Silicon increased the presence of δ-ferrite which promoted densification during sintering. An addition of 3 mass % Si resulted in a tensile strength of 540 MPa with 30% elongation at fracture, while 5 mass % increased tensile strength to 780 MPa with 11% elongation. Silicon addition above 5 mass % resulted in severe dimensional change and distortion.

The corrosion resistance of conventional sintered stainless steel is inherently inferior to that of its wrought counterpart because of the existence of porosity. Factors affecting corrosion behavior of sintered austenitic stainless steel in different environments have been investigated by various authors [13–16].

0022–2461/89 $03.00 + .12

In the present investigation up to 2 and 5 mass % phosphorus and silicon, respectively, were added by a premix route to both γSS and its 4 vol % Y_2O_3-containing composites, and sintered properties such as densification behaviour, mechanical properties and corrosion resistance were evaluated.

2. Experimental details

The characteristics of different powders used in the present investigation are given below.

Type 316L stainless steel prealloyed powder (water atomized)

Source: SCM Glidden metals, Ohio, USA.

Chemical composition: C 0.024%
Si 0.85%
Mn 0.24%
S 0.019%
Cr 16.79%
Mo 2.07%
Ni 13.50%
Fe balance

Physical properties: apparent density 2.70 Mg m^{-3}
flow rate 30 sec/50 g

Sieve analysis (Taylor): +100 0.4%
+150 7.6%
+200 16.1%
+325 29.9%
−325 46.0%

Yttria powder

Source: Rare Earth Products Ltd, UK.

Chemical composition: Y_2O_3 99.9%
Al 1 p.p.m.
Ca 10 p.p.m.
Mg 1 p.p.m.
Si 10 p.p.m.

Apparent density: 0.78 Mg m^{-3}

Flow rate: no free flow

Average particle size: 2.9 μm (FSSS)

Silicon powder

Source: Metal Powder Company Ltd, Madurai, India.

Chemical composition: Si 98.1%
SiO_2 1.9%

Average particle size: 9.0 μm (FSSS)

Iron-phosphorus master alloy (Fe_3P)

Source: Hoganas AB, Sweden.

Chemical composition: P 16%
Fe balance

Apparent density: 1.8 Mg m^{-3}

Flow rate: no free flow

Particle size: −325 mesh

Type 316L austenitic stainless steel (γSS) and 4 vol % Y_2O_3 powder were manually mixed in a mortar and pestle followed by an additional mixing for 1 h in a laboratory-type double-cone blender (Netzsch). Fe_3P master alloy powder corresponding to up to 2 mass % phosphorus and up to 5 mass % silicon powder were mixed for 30 min with straight γSS or its 4 vol % Y_2O_3-containing premix. Cylindrical green compacts of 1.28 × 10^{-2} m diameter and approximately 0.8 × 10^{-2} m height were made from the powder premixes in a single-acting hydraulic press at a compaction pressure of 700 MPa. MPIF tensile test specimens were also made from similar powder premixes, but using a compaction pressure of 500 MPa. The green cylindrical and MPIF tensile test specimens were sintered in hydrogen in a laboratory-type silicon carbide heated tubular furnace. The sintering temperatures of 1100 and 1300° C (± 5° C) for cylindrical compacts and 1300 ± 5° C for MPIF tensile test specimens were selected. A sintering period of 1 h was maintained in all cases. The dew point of hydrogen was measured on Shaw Automatic Dew Point Meter, SADP, which gave a value of −32° C.

Densities were calculated from dimensional measurements and mass of the compacts in green and sintered conditions. They were also measured by a xylene impregnation method and practically less than 5% difference was observed in densities measured by these two methods.

The densification parameter (ΔD) was calculated from

$$\Delta D = \frac{\text{sintered density} - \text{green density}}{\text{theoretical density} - \text{green density}}$$

Optical micrographs of polished surfaces of the sintered compacts, after etching with Marbles' reagent, were taken at a magnification of × 200.

The hardness of the sintered compacts was measured on a Vickers Hardness Testing machine, Model HPO 250 (Fritz Heckert, Leipzig) using a load of 5 kg (49 N). Tensile testing of the sintered MPIF samples was carried out on an Instron machine (Instron Model 1195) of 9.8 × 10^4 N capacity.

The as-sintered cylindrical compacts were immersed in 250 ml 1 N H_2SO_4 test solution at room temperature and left undisturbed for 24 h and 360 h, respectively. The per cent mass loss per unit area of the corroding samples was calculated by weighing these specimens

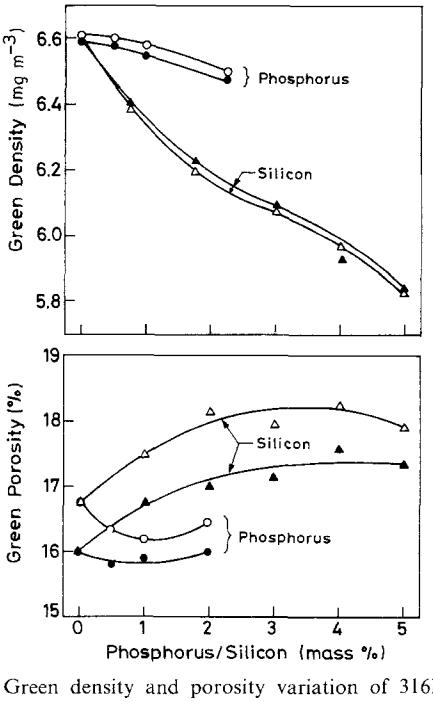

Figure 1 Green density and porosity variation of 316L and its 4 vol % Y_2O_3-containing compacts with phosphorus and silicon addition.

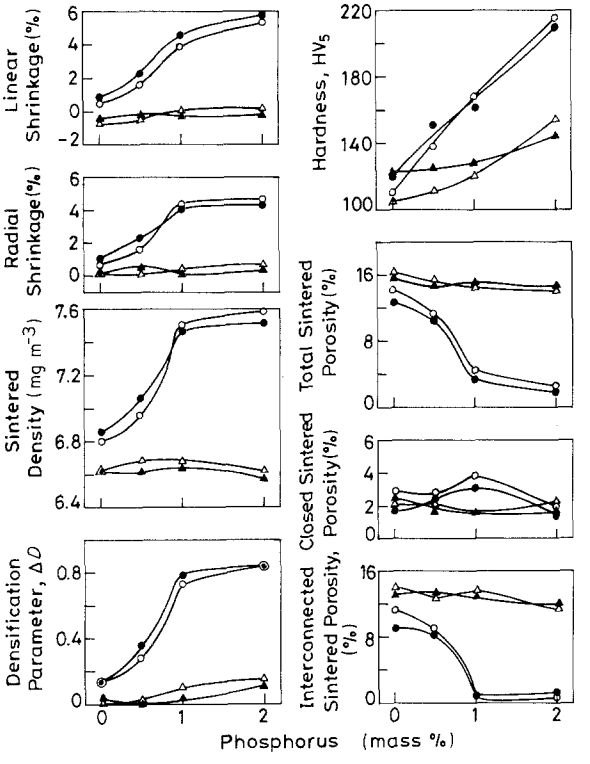

Figure 2 Properties variation of 316L and its 4 vol % Y_2O_3 containing composites with phosphorus content after sintering at 1100 and 1300° C for 1 h in hydrogen. (○) 316L, 1300° C; (△) 316L, 1100° C; (●) 316L–4 vol % Y_2O_3, 1300° C; (▲) 316L–4 vol % Y_2O_3, 1100° C.

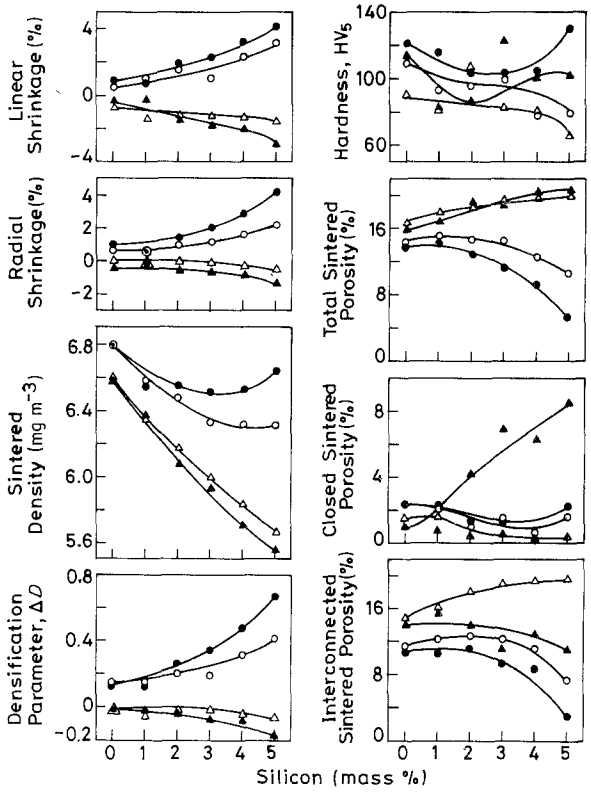

Figure 3 Properties variation of 316L and its 4 vol % Y_2O_3-containing composites with silicon content after sintering at 1100 and 1300° C for 1 h in hydrogen. (○) 316L, 1300° C; (△) 316L, 1100° C; (●) 316L–4 vol % Y_2O_3, 1300° C; (▲) 316L–4 vol % Y_2O_3, 1100° C.

before and after the corrosion test and also knowing the surface area of the as-sintered specimens.

An X-ray diffractometer model Iso-Bebyeflex, 2002D (Rich Seifert, West Germany) was used for quantitative analysis of ferrite and austenite in sintered cylindrical compacts containing 2 mass % phosphorus and 5 mass % silicon.

3. Results

The effects of additive and matrix hardness on the green density of compacts are such that silicon addition lowers the green density more drastically than phosphorus addition (Fig. 1). The presence of Y_2O_3 particles appears to have no appreciable effect on the green density values.

The densification behaviour of straight γSS is inferior compared to its composites containing Y_2O_3 (Fig. 2). This feature is more predominant after sintering at 1300° C compared to 1100° C, in either case.

Fig. 3 shows that the shrinkages and densification parameter were found to decrease with increasing silicon content of the compacts after 1100° C sintering. The difference in the densification behaviour of γ_{SS} and its Y_2O_3-containing composites increased with increasing silicon content. Higher densification is observed in the case of Y_2O_3-containing compacts, compared to the straight γ_{SS} after sintering at 1300° C for any silicon addition. However, a reverse trend is noticed when the compacts were sintered at 1100° C.

From the microstructures (Fig. 4) it is quite obvious that pore rounding took place and these pores were more concentrated at grain boundaries in the case of phosphorus addition. In the case of silicon addition, pore rounding is not prominent. However, Y_2O_3 showed a positive result on pore rounding for both additives.

Ultimate tensile strength (UTS) and per cent elongation values improved up to 1 mass % P and 4 mass % S, beyond which a decreasing trend was observed (Fig. 5). In the case of silicon addition, the tensile strength values were higher than those for straight γSS. However, the trend was reversed in the case of phosphorus addition.

Hardness values increased linearly with increasing phosphorus content when sintered at 1100 or 1300° C, for either straight γSS or its 4 vol % Y_2O_3-containing composites. In general, hardness values were higher for Y_2O_3-containing composites compared to straight γSS sintered at either temperature.

It is clear from Table I that γSS containing 5 mass % Si showed the presence of both ferrite and austenite but in the case of 2 mass % Si only austenite was observed. In the case of γSS–2 mass % P only 3 vol % ferrite could be detected.

Microhardness on duplex stainless steel, i.e. 316L–5% Si, was observed to be 183 and 237 for austenite and ferrite phases, respectively, whereas the average

TABLE I Volume fraction of different phases in sintered 316L stainless steel containing phosphorus and silicon. Sintered at 1300° C for 1 h in hydrogen

Composition	δ-ferrite (vol %)	Austenite (vol %)
316L	0	100
316L–2% P	3	97
316L–2% Si	Not detected	100
316L–5% Si	15	85

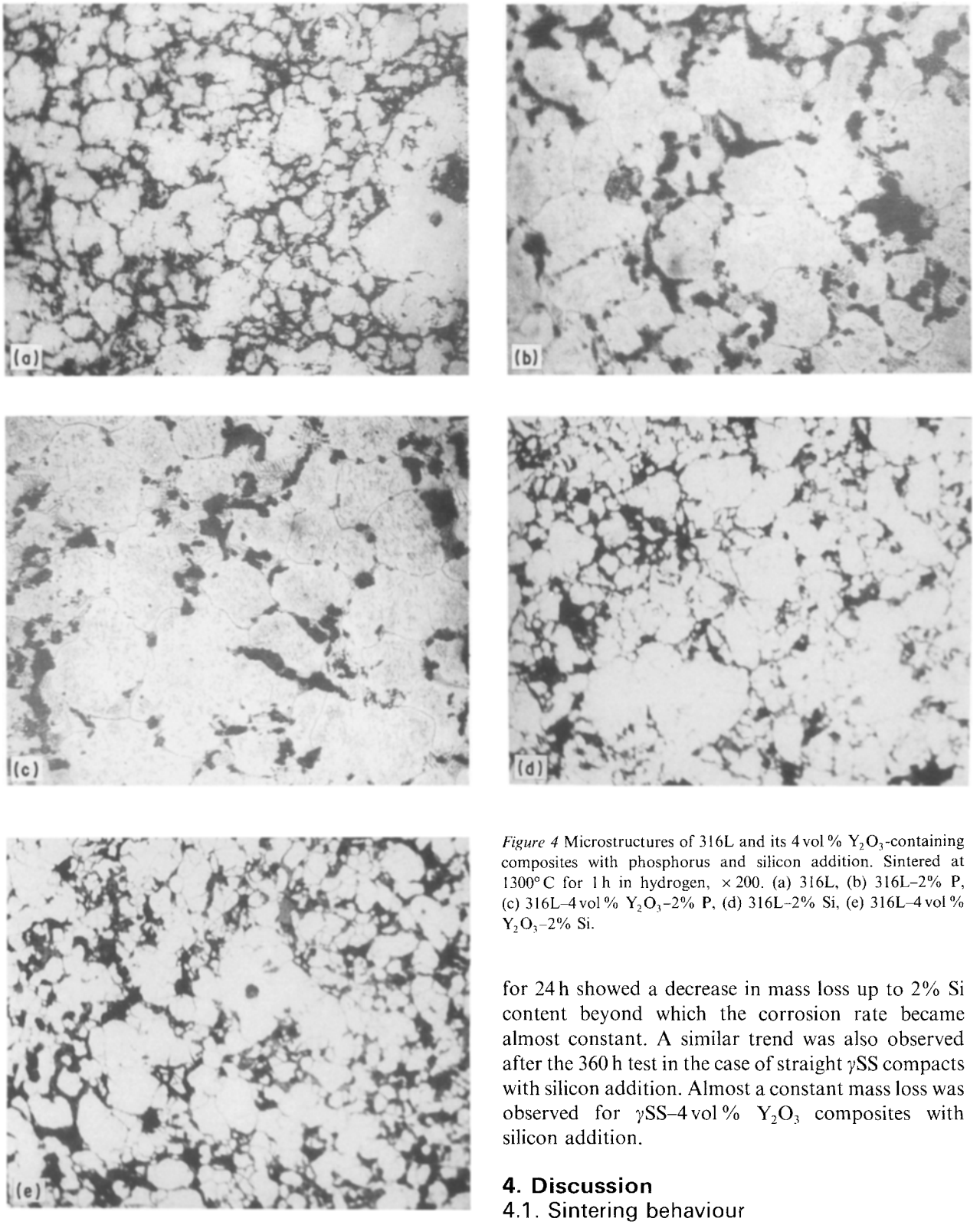

Figure 4 Microstructures of 316L and its 4 vol % Y_2O_3-containing composites with phosphorus and silicon addition. Sintered at 1300° C for 1 h in hydrogen, × 200. (a) 316L, (b) 316L–2% P, (c) 316L–4 vol % Y_2O_3–2% P, (d) 316L–2% Si, (e) 316L–4 vol % Y_2O_3–2% Si.

microhardness on 316L-2% P alloy was found to be 314.

Fig. 6 shows that the mass loss as a result of corrosion is almost identical for either straight γSS or its composites, tested for 24 h for any phosphorus content. However, a minimum mass loss is observed at 1 mass % phosphorus in either alloy. Mass loss variation in sintered compacts tested for 360 h in 1 N H_2SO_4 does not show any specific relation either with increasing phosphorus content or with total sintered porosity of the compacts. Fig. 7 shows that the compacts tested for 24 h showed a decrease in mass loss up to 2% Si content beyond which the corrosion rate became almost constant. A similar trend was also observed after the 360 h test in the case of straight γSS compacts with silicon addition. Almost a constant mass loss was observed for γSS–4 vol % Y_2O_3 composites with silicon addition.

4. Discussion

4.1. Sintering behaviour

The present results reveal that compacts sintered at 1100° C practically exhibit no improvement in densification with increase in phosphorus content in either straight γSS or its 4 vol % Y_2O_3-containing composites (Fig. 2). This may be attributed to the insignificant liquid-phase sintering allowed at this lower temperature [19]. The binary Fe–P phase diagram (Fig. 8) reveals the presence of two eutectic reactions at 1049 and 1264° C apart from a peritectic reaction at 1168° C. The eutectic melt is redistributed by capillary forces [20], thus providing for favourable conditions for the diffusion of phosphorus into the 316L particles. In the present alloy system, i.e. 316L, there is a

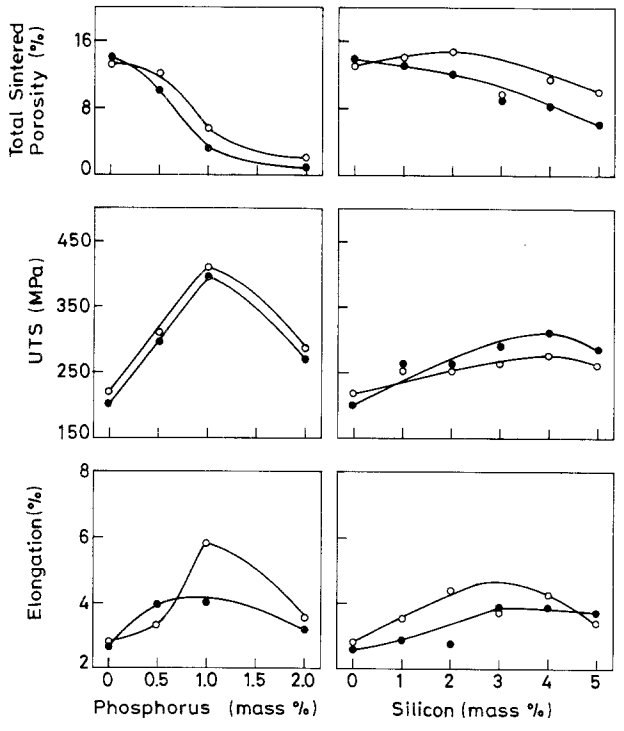

Figure 5 UTS and per cent elongation variation of (○) 316L and (●) its 4 vol% Y_2O_3-containing composites with increase in phosphorus/silicon content after sintering at 1300° C for 1 h in hydrogen.

high solute content in the iron matrix and an over-simplification of the liquid-phase formation is highly uncertain at 1100° C. The results on sintering carried out at 1300° C show that up to 1 mass % P addition, linear and radial shrinkages, sintered density and densification parameters were sharply increased. Beyond this level of phosphorus the properties variations are not so drastic.

The general improvement in overall densification behaviour of silicon-containing 316L alloys after 1300° C sintering, unlike the 1100° C sintering, is attributed to the transient liquid-phase formation. The binary phase diagram of the Fe–Si system (Fig. 8) shows the presence of a eutectic melt at 1190 and 1202° C with 19% and 22% Si, respectively. With increase in silicon content, the probability of the formation of a eutectic melt at the particle–particle contacts will be higher. Further, interdiffusivity of component atoms is relatively higher at the elevated temperature of sintering, i.e. at 1300° C.

Phosphorus and silicon are both ferrite stabilizers in steel, the latter having a pronounced effect [9]. In the case of 1300° C sintering, the liquid formation of Fe_3P is complete, whereas at this temperature, full utilization of liquid-phase sintering in the 316L–Si system could not be exploited. This is evinced by the sintered porosity variations (Figs 2 and 3) such that the phosphorus-containing steel possessed a lower sintered porosity than a steel containing equivalent silicon. After X-ray studies the ferrite content in the 5 mass % Si-containing stainless steel was found to be 15 vol % compared to 3 vol % in 2 mass % Ph-containing alloy. This suggests that although the volume percent of liquid was not appreciable, the diffusivity of the silicon in the matrix was high enough to give as much as 15 vol % ferrite. It also appears that the ferrite stabilization is not a direct function of the amount of silicon content, because the X-ray diffraction study on 2 mass % Si-containing alloy did not show the presence of any ferrite.

The higher densification of Y_2O_3-containing composites compared to the straight γSS may be attributed to better bonding between the dispersoid and the matrix because of chemical interaction [21]. It is probable that the presence of Cr_2O_3 in the steel would promote such an interaction through the formation of compound $YCrO_3$ [22].

In general, porosity has a large effect on sintered properties and microstructures, and the strength tends to be one of the less sensitive monitors. The absence of clear-cut correlation between mechanical properties and porosity level beyond 1 mass % P may be attributed to the above reasons.

The gradual increase in the sintered properties after 1300° C for γSS or its Y_2O_3-containing composites with increase in silicon content is attributed to a

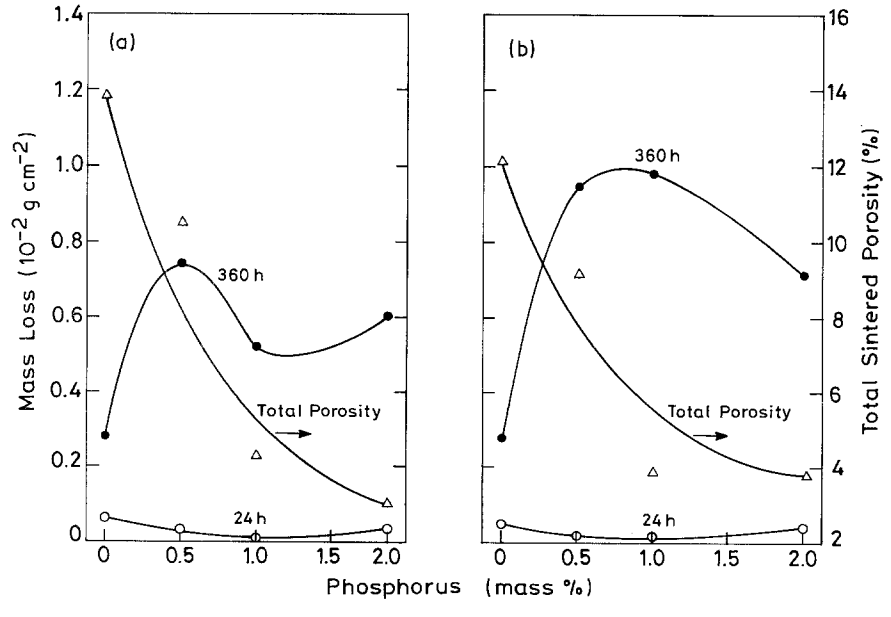

Figure 6 Mass loss variation of (a) 316L and (b) its 4 vol % Y_2O_3-containing composites with phosphorus content in 1 N H_2SO_4 for two different periods, i.e. 24 and 360 h (sintered at 1300° C for 1 h in hydrogen).

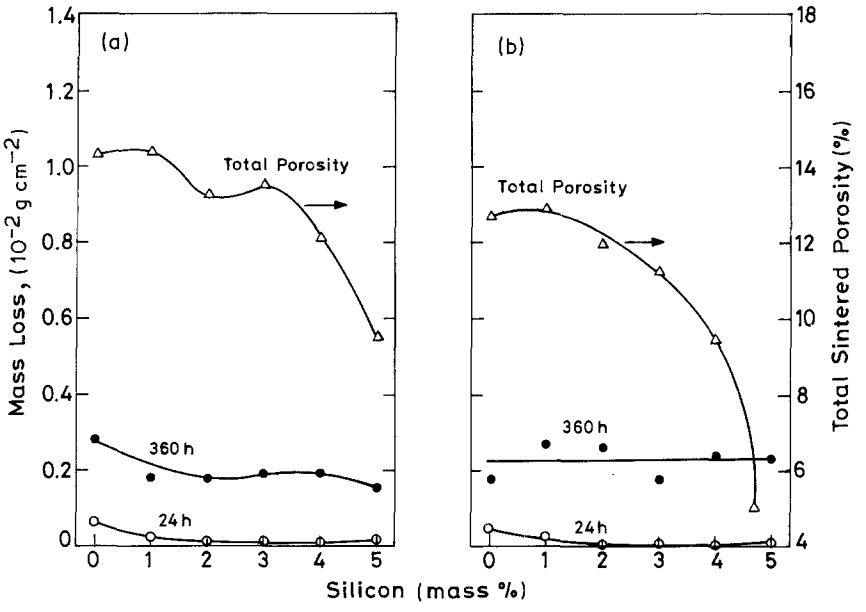

Figure 7 Mass loss variation of (a) 316L and (b) its 4 vol % Y_2O_3-containing composites with silicon content in 1 N H_2SO_4 for two different periods, i.e. 24 and 360 h (sintered at 1300° C for 1 h in hydrogen).

lowering of the total sintered porosity. The improved mechanical properties of γSS–Y_2O_3–Si composites compared to the straight γSS–Si composites is due to the chemical interaction between Y_2O_3 dispersoids and 316L matrix, as discussed elsewhere [22].

The solid solution hardening effect of phosphorus in iron is known to be greater than that of silicon. This feature is manifested in the present results. A better ductility for phosphorus-containing alloys than that for silicon-containing ones is the natural outcome of a larger volume fraction of the liquid phase during sintering of the former, which lowers the sintered porosity values.

4.2. Corrosion behaviour

The corrosion behaviour of 316L and its 4 vol % Y_2O_3-containing composites (Fig. 7), shows no definite relation between corrosion resistance and total sintered porosity with increasing phosphorus content. With the increase in the silicon content in straight γSS sintered compacts tested for either 24 or 360 h, a slight improvement in the corrosion resistance may be attributed to the decrease in porosity level after silicon addition (Fig. 7).

5. Conclusions

1. Sintering of 316L stainless steel or its Y_2O_3-

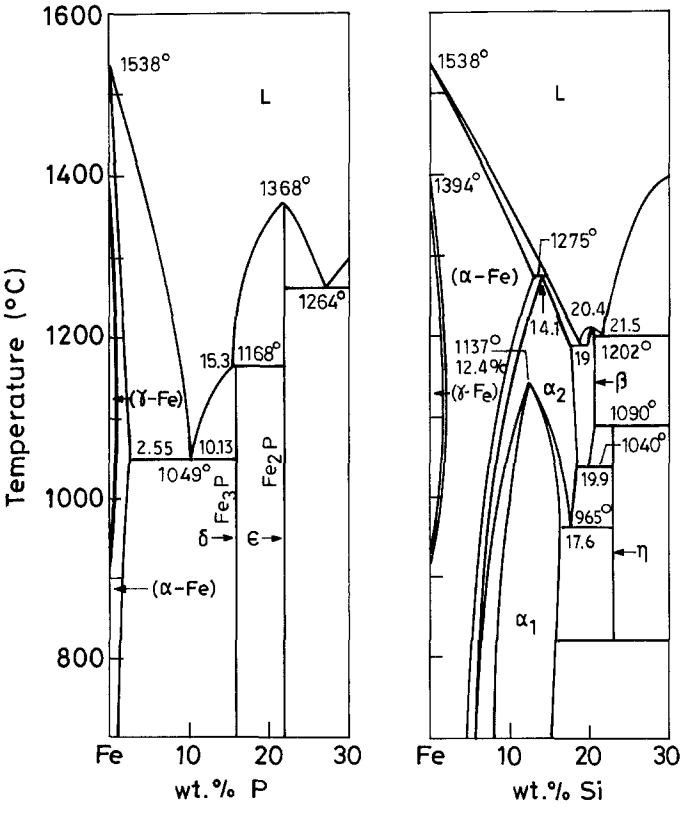

Figure 8 Binary phase diagrams of Fe–P and Fe–Si systems.

containing composites, when carried out at 1100° C, shows shrinkage in compacts containing phosphorus, while the reverse trend was noticed in the case of silicon addition. Similar compacts sintered at 1300° C, show shrinkage with increase of either phosphorus or silicon content. The improvement in densification was more pronounced in the case of phosphorus addition than the silicon addition.

2. Optimum ultimate tensile strength and percent elongation were observed at 1 mass % P or at 4 mass % Si in straight 316L or its Y_2O_3-containing composites.

3. The effect of phosphorus addition on solid solution hardening is much more pronounced, whereas the silicon addition does not show hardening. However, microhardness measurements did confirm the hardening role of silicon in the ferrite phase.

4. Silicon addition imparts better corrosion resistance in a 1 N H_2SO_4 environment compared to the phosphorus addition. Y_2O_3-containing composites show better resistance than the straight 316L.

References

1. R. M. GERMAN, "Powder Metallurgy Science" (MPIF, Princeton, New Jersey, 1984).
2. R. DUCKETT and D. A. ROBINS, *Metallurgica* **74** (444) (1966) 163.
3. G. HOFFMANN, F. THUMMLER and G. ZAPF, in "Powder Metallurgy – Third European P/M Symposium", Conference Supplement part I (1971) p. 335.
4. F. V. LENEL, "Powder Metallurgy – Principles and Applications" (MPIF, Princeton, New Jersey, 1980).
5. S. K. MUKHERJEE and G. S. UPADHYAYA, *High Temp. Technol.* **1** (1983) 229.
6. I. A. WHITE, in "Stainless Steel Powder Seminar", Detroit, February 1965 (Hoganas Corporation, New Jersey, p. 47).
7. "Metals Handbook", Vol. 8 (ASM, Ohio, 1973).
8. R. L. SANDS and J. F. WATKINSON, *Powder Metall.* **9** (5) (1966) 85.
9. N. B. SHAW and R. W. K. HONEYCOMBE, *ibid.* **20** (4) (1977) 191.
10. W. F. WANG and Y. L. SU, *ibid.* **29** (4) (1986) 269.
11. *Idem, ibid.* **29** (3) (1986) 177.
12. WANG WEN-FENG, "Proceedings P/M-82 in Europe", Florence, Italy, 20–25 June, 1982, Associazione Italiano di Metallurgia, Milano, p. 756.
13. R. L. SANDS, G. F. BIDMEAD and D. A. OLIVER, in "Modern Developments in Powder Metallurgy", edited by H. H. Hausner, Vol. 2 (Plenum, New York, 1966) p. 73.
14. G. LEI, R. M. GERMAN and H. S. NAYAR, *Powder Metall. Inter.* **15** (2) (1980) 70.
15. D. H. RO and E. KLAR, in "Modern Developments in Powder Metallurgy", edited by H. H. Hausner, Vol. 13 (Plenum, New York, 1981) p. 247.
16. G. WARNGLEN, "An Introduction to Corrosion and Protection of Metals" (Institut for Metall Skydel, Stockholm, 1972) p. 82.
17. G. ARTHUR, *J. Inst. Metals* **83** (1954–55) 329.
18. C. J. SMITHELLS (ed.), "Metals Reference Book", Vol. III (Butterworths, London, 1967) p. 696.
19. V. N. EREMENKO *et al.*, "Liquid Phase Sintering" (Consultants Bureau, New York, 1970) p. 4 (translated from Russian).
20. P. LINDSKOG *et al.*, in "Modern Developments in Powder Metallurgy, edited by H. H. Hausner, Vol. 10 (MPIF, New Jersey, 1977) p. 97.
21. S. LAL and G. S. UPADHYAYA, *J. Powder Bulk Solid Technol.* **11**(3) (1987) 1–2.
22. S. LAL and G. S. UPADHYAYA, *J. Mater. Sci. Lett.* **6** (1987) 761.

Received 1 February
and accepted 11 October 1988